Biology of Reproduction, 2017, 96(5), 993–1006
doi:10.1093/biolre/iox029
Research Article
Advance Access Publication Date: 18 April 2017

OXFORD

Research Article

IFT25, an intraflagellar transporter protein dispensable for ciliogenesis in somatic cells, is essential for sperm flagella formation†

Hong Liu[1,2], Wei Li[2], Yong Zhang[2,3], Zhengang Zhang[2,4], Xuejun Shang[5], Ling Zhang[1,2], Shiyang Zhang[1,2], Yanwei Li[6], Andres V Somoza[7], Brandon Delpi[8], George L Gerton[9], James A Foster[8], Rex A Hess[10], Gregory J Pazour[11] and Zhibing Zhang[1,2,*]

[1]School of Public Health and Hubei Province Key Laboratory of Occupational Hazard Identification and Control, Wuhan University of Science and Technology, Wuhan, Hubei, China; [2]Department of Obstetrics and Gynecology, Virginia Commonwealth University, Richmond, Virginia, USA; [3]Department of Dermatology, Tongji Medical College, Huazhong University of Science and Technology, Wuhan, China; [4]Department of Gastroenterology, Tongji Hospital, Tongji Medical College, Huazhong University of Science and Technology, Wuhan, Hubei, China; [5]Department of Andrology, Jinling Hospital, Nanjing University, School of Medicine, Nanjing, China; [6]Department of Computer Science, Wellesley College, Wellesley, Massachusetts, USA; [7]Department of Humanities and Sciences, Honor College, Virginia Commonwealth University, Richmond, Virginia, USA; [8]Department of Biology, Randolph-Macon College, Ashland, Virginia, USA; [9]Center for Research on Reproduction and Women's Health Perelman School of Medicine, University of Pennsylvania, Philadelphia, Pennsylvania, USA; [10]Comparative Biosciences, College of Veterinary Medicine, University of Illinois, Urbana, Illinois, USA and [11]Program in Molecular Medicine, University of Massachusetts Medical School, Worcester, Massachusetts, USA

*__Correspondence:__ Department of Obstetrics/Gynecology, Virginia Commonwealth University, 1101 E Marshall Street, Richmond, VA 23298, USA. E-mail: zhibing.zhang@vcuhealth.org

†__Grant Support:__ This research was supported by NIH grant HD076257, HD090306, Virginia Commonwealth University Presidential Research Incentive Program (PRIP) and Massey Cancer Award (to Zhibing Zhang), NIH grant GM060992 (to GJP), Chenery and Rashkind Grants from Randolph-Macon College (JF). Natural Science Foundation of China (81571428, 81300536, 81370750, and 81671514), and Special Fund of Wuhan University of Science and Technology for Master Student's short-term studying abroad. Confocal microscopy and SEM were performed in the VCU Microscopy Facility of Virginia Commonwealth University (5P30NS047463). TEM was performed at Randolph-Macon College (NSF1229184).

Significance Statement: Intraflagellar transport is essential for the assembly and maintenance of most eukaryotic cilia and flagella. Sperm have longer flagella/cilia of than any other mammalian cells. Besides the core "9+2" axoneme structure, the sperm tail has accessory structures, including outer dense fibers and the fibrous sheath. Our study demonstrated that IFT25, an IFT component that is not required for ciliogenesis in primary cilia and motile cilia in the somatic tissues, plays a fundamental role in sperm flagella formation. Our findings suggest that the mechanism of sperm flagella assembly is different from that of somatic cells, and that IFT25 plays a special role in male germ cell development.

Received 27 November 2016; Revised 5 March 2017; Accepted 13 April 2017

Abstract

Intraflagellar transport (IFT) is a conserved mechanism essential for the assembly and maintenance of most eukaryotic cilia and flagella. However, IFT25, a component of the IFT complex, is not required for the formation of cilia in somatic tissues. In mice, the gene is highly expressed in the testis, and its expression is upregulated during the final phase when sperm flagella are formed.

To investigate the role of IFT25 in sperm flagella formation, the gene was specifically disrupted in male germ cells. All homozygous knockout mice survived to adulthood and did not show any gross abnormalities. However, all homozygous knockout males were completely infertile. Sperm numbers were reduced and these sperm were completely immotile. Multiple morphological abnormalities were observed in sperm, including round heads, short and bent tails, with some tails showing branched flagella and others with frequent abnormal thicknesses, as well as swollen tips of the tail. Transmission electron microscopy revealed that flagellar accessory structures, including the fibrous sheath and outer dense fibers, were disorganized, and most sperm had also lost the "9+2" microtubule structure. In the testis, IFT25 forms a complex with other IFT proteins. In *Ift25* knockout testes, IFT27, an IFT25 binding partner, was missing, and IFT20 and IFT81 levels were also reduced. Our findings suggest that IFT25, although not necessary for the formation of cilia in somatic cells, is indispensable for sperm flagellum formation and male fertility in mice.

Key words: intraflagellar transport, ciliogenesis, germ cells, spermiogenesis, flagellogenesis.

Introduction

The cilium or flagellum is a cell organelle supported by a microtubular scaffold, the axoneme, and is surrounded by a membrane that is continuous with the cell's plasma membrane but is specialized in protein and lipid content [1–3]. Cilia and flagella protrude from the surface of many eukaryotic cells and have various functions ranging from cell locomotion to the sensing of environmental stimuli [4, 5]. As evolutionarily conserved cellular appendages, cilia and flagella are assembled and maintained by a motility process called intraflagellar transport (IFT), which was first discovered in the unicellular green algae *Chlamydomonas* [6]. IFT involves a pool of large nonmembrane-bound protein complexes, termed IFT particles, that lie in close proximity to the basal body and move from the base to the tip of the flagellum, and then back to the base [7, 8]. The IFT machinery comprises IFT-A and IFT-B protein complexes, which contain at least six and sixteen polypeptides, respectively. Those IFT particles are thought to carry precursors needed for ciliary/flagellar assembly from the site of synthesis in the cell body to the site of assembly in the cilium/flagellum, and the IFT complexes serve as adaptors to mediate contacts between cargo proteins and motors. Although these complexes are thought to travel together, different members of each complex have been proposed to serve broadly distinctive roles [8].

Among the IFT genes, *Ift25* is of particular interest. IFT25 is conserved in many but not all ciliated eukaryotes. It is well conserved throughout the vertebrates and is also present in some invertebrates such as urchins, anemones, and *Trichoplax*. *Ift25* is not found in many model organisms such as plants, *Saccharomyces*, *Caenorhabditis*, *Drosophila*, or *Plasmodium*, but is conserved in *Chlamydomonas* and there are distant homologs in the parasitic protozoa *Leishmania* and *Trypanosoma* [9].

Mouse IFT25 was identified in an effort to characterize mouse IFT complex B components [10, 11]. Its homolog, *C1orf41*, a human IFT27/Rabl4-binding protein [12], was first identified as a salt-extractable protein from placenta and named pp25 [13], and was later described as a small heat shock protein [14, 15] and called Hspb11, Hsp16.2, and HSPCO34. Subsequent coimmunoprecipitation (co-IP) assay confirmed that mouse IFT25 is present in the same complex with other mouse IFT B components and is localized in the cilium and centriole in transfected mammalian cells [10]. The IFT25 ortholog in *Chlamydomonas*, FAP232, was identified in an effort to study uncharacterized putative flagellar proteins [16]. FAP232 showed a spotted distribution along the flagellum and an accumulation at the basal bodies. This pattern is characteristic for IFT proteins. FAP232 colocalized with the IFT protein IFT46 and cosedimented with IFT particles in sucrose gradients. Furthermore, FAP232 was coimmunoprecipitated with IFT complex B protein IFT46, but not with IFT complex A protein IFT139. Thus, FAP232 is a novel component of IFT complex B and has been renamed IFT25 [16]. Further studies demonstrated that *Chlamydomonas* IFT25 is a phosphoprotein. Like human IFT25, *Chlamydomonas* IFT25 also binds to *Chlamydomonas* IFT27, and the two proteins colocalize at the distal-most portion of basal bodies, probably the transition zones, and concentrate in the basal body region by partially overlapping with other IFT complex B subunits, such as IFT46. In flagella, the majority of IFT27 and IFT25 including both phosphorylated and nonphosphorylated forms are cosedimented with other complex B subunits in the 16S fractions. In contrast, in cell bodies, only a fraction of the IFT25 and IFT27 proteins are integrated into the preassembled complex B, and IFT25 detected in complex B is preferentially phosphorylated [17].

The crystal structure of *Chlamydomonas reinhardtii* IFT25/27 revealed that IFT25 and IFT27 interact via a conserved interface. IFT27 displays the fold of Rab-like small guanosine triphosphate hydrolases (GTPases), binds GTP and GDP with micromolar affinity, and has very low intrinsic GTPase activity, suggesting that it likely requires a GTPase-activating protein (GAP) for robust GTP turnover. A patch of conserved surface residues contributed by both IFT25 and IFT27 is found adjacent to the GTP-binding site and could mediate the binding to other IFT proteins as well as to a potential GAP [18].

To study the role of IFT25 in mammals, *Ift25* knockout (KO) mice were generated. *Ift25* KO die at birth with multiorgan structural birth defects, including abnormal skeletons, structural heart, and lung disease. It is not required for cilia assembly in MEFs and tracheal epithelial cells; however, *Ift25* KO have Hedgehog signaling defects within the primary cilia. In MEFs, most of the IFT subunits, including IFT88, 57, 20, 140, were not significantly affected by the loss of IFT25, IFT27 was strongly depleted [19]. IFT25 is also not required for ciliogenesis in skin, but is essential for hedgehog signaling during hair follicle morphogenesis [20].

Given that genes encoding IFT25 homologs are absent from the genomes of organisms that lack cilia and flagella and, interestingly, also from those of *Drosophila melanogaster* and *Caenorhabditis elegans*, it is likely that IFT25 has a specialized role in IFT that is not required for the assembly of cilia or flagella in the worm and fly. This also seems to be true for mammals, as mouse IFT25 is also not required for ciliogenesis for MEFs, skin, and tracheal epithelial cells [19, 20]. To explore if this is a general phenomenon,

particularly for sperm flagella, which have the longest motile axonemal structures in vivo, we inactivated *Ift25* gene in male germ cells and investigated the role of IFT25 in mouse flagella formation and male fertility. To our surprise, silencing the *Ift25* gene in male germ cells resulted in severe spermatogenesis defects and male infertility, associated with dramatically reduced sperm number and disrupted sperm flagellar structures. The developed sperm completely lacked motility, and most lost "9+2" axoneme structure and had some abnormal accessory structures including missing outer dense fibers and disorganized fibrous sheath (FS). Some sperm flagella also lost cell membranes and some sperm had branched flagella. In the *Ift25* mutant mice, IFT27, an IFT25 binding partner, was missing from the testis, and expression levels of other IFT proteins IFT20 and IFT81 were also reduced. Our findings suggest that IFT25, even though not necessary for cilia formation in the somatic tissues, is essential for sperm flagella formation, normal spermiogenesis, and male fertility in mice. Our studies strongly suggest that IFT25 has a different role in male germ cells compared to other somatic cells.

Materials and methods

Ethics statement

All animal work was approved by Virginia Commonwealth University's Institutional Animal Care and Use Committee (protocol AD10000167) in accordance with federal and local regulations regarding the use of nonprimate vertebrates in scientific research.

Generation of germ cell-specific *Ift25* knockout mice

Ift25$^{flox/flox}$ mice were generated previously by Dr. Gregory J. Pazour, University of Massachusetts Medical School [19], and *Stra8-iCre* mice were purchased from the Jackson Laboratory (Stock No: 008208). Transgenic mouse line *Stra8-cre* expresses improved Cre recombinase under the control of a 1.4 Kb promoter region of the germ cell-specific stimulated by retinoic acid gene 8 (*Stra8*) [21]. To generate the germ cell-specific *Ift25* KO mouse model, the same breeding strategy to generate germ cell-specific *Ift20* mice was used [22]. Briefly, 3–4-month-old *Stra8-cre* males were crossed with 3–4-month-old *Ift25*$^{flox/flox}$ females to obtain *Stra8-iCre; Ift25*$^{flox/+}$ mice. The 3–4-month-old *Stra8-iCre; Ift25*$^{flox/+}$ males were crossed back with 3–4-month-old *Ift25*$^{flox/flox}$ females again, and the *Stra8-iCre; Ift25*$^{flox/flox}$ were considered to be the homozygous KO mice, and *Stra8-iCre; Ift2*$^{flox/+}$ mice were used as the controls.

To genotype the offspring, genomic DNA was isolated as described previously [19]. The following primers were used for genotyping: *Stra8-iCre* forward: 5′-GTGCAAGCTGAACAA CAGGA-3′; *Stra8-iCre* reverse: 5′-AGGGACACAGCATTGGAGTC-3′, and *Ift25* genotypes were determined as described as previously [19].

Real-time PCR

Total tissue RNA was isolated using TRIZOL reagent (QIAGEN), and cDNA was synthesized using a first strand cDNA SensiFASTTM cDNA Synthesis Kit (BIOLINE). To compare *Ift25* mRNA expression levels in different mouse tissues, real-time fluorescence quantitative PCR (qPCR) was conducted using the following primer pair designed with GeneScript tools: forward: 5′-CACCGAAGAGGCTAACCATT-3′, and reverse: 5′-GATGTGGCCAGAATCACTTC-3′. Mouse *Gapdh* was used to normalize the expression level.

Assessment of fertility and fecundity

To test fertility and fecundity, KO and control males (6 weeks old or 3–4 months old) were paired with wild-type females (3–4 months old) for 3 months. Mating cages typically consisted of one male and one female. Mating behavior was observed, and the females were checked for the presence of vaginal plugs and pregnancy. Once pregnancy was detected, the females were put into separate cages. The number of mice achieving a pregnancy and the number of pups from each mating set or pregnancy were recorded.

Western blot analysis

Tissue samples were homogenized in lysis buffer [(50 mM Tris–HCl pH 8.0, 170 mM NaCl, 1% NP40, 5 mM EDTA, 1 mM DTT and protease inhibitors (Complete mini; Roche diagnostic)] using Ultra Turrax and centrifuged at 13 000 rpm, for 10 min at 4°C. Protein concentrations were measured using Bio-Rad DCTM protein assay kit (Bio-Rad). Samples were separated by sodium dodecyl sulfate-polyacrylamide gel electrophoresis and subsequently electrotransferred onto polyvinylidene difluoride membranes (Millipore, Billerica, MA, USA). The membranes were then blocked in a Tris-buffered saline (TBST) solution containing 5% nonfat dry milk powder and 0.05% Tween 20 (TBST), and incubated with indicated antibodies (IFT25-1: 1:2000, Cat No: 15732-1-AP, ProteinTech; IFT25-2: 1:1000, Cat No: MBS2519685, My BioSource; IFT25-3: 1:1000, Cat No: bs-9798R, Bioss; IFT74: 1:1000, Cat No: AAS27620e, from ANTIBODY VERIFY; IFT81: 1:1000, Cat No: 11744-1-AP, ProteinTech; β-actin: 1:2000, Cat No: 4967S, Cell Signaling; Antibodies against IFT20, IFT27 and IFT140 (1:2000) were from Dr. Pazour's laboratory [19, 23, 24] Table 1) at 4°C overnight. After washing three times with TBST, the membranes were incubated with the secondary antibody conjugated with horseradish peroxidase with dilution of 1:2000 at room temperature for 1 h. Followed by washing with TBST twice and last washing with TBS, the bound antibodies were detected with Super Signal Chemiluminescent Substrate (Pierce, Rockford, IL, USA).

Direct yeast two-hybrid experiment

To detect interaction between mouse IFT25 and mouse IFT27, full-length mouse *Ift25* and *Ift27* cDNAs were amplified using the following primers: IFT25forward: 5′-GAATTCATGAGG AAAGTGGATCTCTGC-3′, and IFT25reverse: 5′-GGATCCCTAAGGAAGACTTGAGACT G-3′; and IFT27forward: 5′-CATATGGTGAAGCTAGCTGCCAAATG-3′, and IFT27reverse: 5′-GGATCCCTCACACCAGGGTATGGAAT-3′. After sequencing, the two cDNAs were cloned into pGADT7 and pGBKT7. IFT25/pGADT7 and IFT27/pGBKT7 or IFT25/pGBKT7 and IFT27/pGADT7 were cotransformed into the AH109 host strain using the Match-Maker two-hybrid System 3 (Clontech) according to the manufacturer's instructions. Two plasmids containing simian virus (SV) 40 large T antigen (LgT) in pGADT7 and p53 in pGBKT7 were cotransformed into AH109 and used as positive controls. Expression of both proteins (IFT25 and IFT27) was analyzed by western blot. The AH109 transformants harboring both IFT25/pGBKT7 (or IFT25/pGADT7) and IFT27/pGADT7 (or IFT27/pGBKT7) were streaked out in complete drop-out medium (SCM) lacking tryptophan, leucine, and histidine to test for histidine prototrophy.

Table 1.

Name	Catalogue number	Purpose	Dilution
Anti-IFT25-1	Protein Tech, 15732-1-AP	Western Blot, co-IP	1:2000 for Western blot; 1μg antibody/mg tissue for IP
Anti-IFT25-2	My BioSource, MBS2519685	Western Blot	1:1000
Anti-IFT25-3	Bioss, bs-9798R	Western Blot	1:1000
Anti-IFT74	Antibody Verify, AAS27620e	Western Blot	1:1000
Anti-IFT81	Protein Tech, 11744-1-AP	Western Blot	1:1000
β-actin	Cell Signaling	Western Blot	1:2000
Anti-IFT20	Dr. Pazour's laboratory	Western Blot	1:2000
Anti-IFT27	Dr. Pazour's laboratory	Western Blot, co-IP	1:2000 for Western blot; 1μl/mg tissue for IP
Anti-IFT140	Dr. Pazour's laboratory	Western Blot	1:2000

Coimmunoprecipitation

Testicular extracts were prepared from adult wild-type mice using an immunoprecipitation (IP) buffer (150 mM NaCl/50 mM Tris-HCl, pH 8.0/5 mM EDTA/1% Triton X-100/1 mM PMSF/proteinase inhibitor mixture). Before IP experiment, the extracts were precleared with protein A beads at 4°C for 30 min. After centrifuging at 12000 rpm for 5 min, the beads were discarded, and the supernatants were used for IP experiment. For each IP experiment, 1 mg of testicular protein was incubated with 1μg of anti-IFT25 (or IFT27) polyclonal antibody (rabbit IgG) or normal rabbit IgG (as a negative control) at 4°C for 2 h, and protein A beads were added with a further incubation period at 4°C overnight. The beads were washed with immunoprecipitation buffer four times, and loading buffer was then added to the beads, which were boiled at 100°C for 10 min; the samples were then processed for western blotting with indicated antibodies.

Histology on tissue sections

Testes and epididymides of adult mice were fixed in 4% formaldehyde solution in Phosphate-buffered saline (PBS), paraffin-embedded, and sectioned into 5 μm slides. Haematoxylin and eosin staining was conducted using standard procedure. Histology was examined using a BX51 Olympus microscope (Olympus Corp., Melville, NY, Center Valley, PA), and photographs were taken with the ProgRes C14 camera (Jenoptik Laser, Germany).

Spermatozoa counting

Sperm cells were collected into warm PBS from cauda epididymides and fixed in 2% formaldehyde for 10 min at room temperature. After washing with PBS, sperm were suspended into PBS again and counted using a hemocytometer chamber under a light microscope, and sperm number was calculated by standard method as we used previously [25].

Spermatozoa motility assay

Sperm motility was evaluated under noncapacitation condition in both PBS and a noncapacitating medium containing the following compounds: NaCl (10 mM), KCl (4.4 mM), KH_2PO_4 (1.2 mM), $MgSO_4$ (1.2 mM), glucose (5.4 mM), pyruvic acid (0.8 mM), lactic acid (2.4 mM), hepes acid (20 mM) [26]. Briefly, epididymal spermatozoa were squeezed out of the cauda epididymis and placed in warm PBS or the noncapacitating medium. Ten minutes after sperm were collected, sperm motility was observed using a Nikon TE200E inverted microscope on a prewarmed slide with SANYO color CCD, Hi-resolution camera (VCC-3972), and Pinnacle Studio HD (Ver. 14.0) software. For each sperm sample, eight fields were analyzed. Individual spermatozoa were tracked using the NIH ImageJ (NIH, Bethesda, MD, USA) and the plugin MTrackJ. Sperm motility was calculated as curvilinear velocity (VCL), which is equivalent to the curvilinear distance (DCL) that is traveled by each individual spermatozoa in one second (VCL = DCL/t).

Transmission electron microscopy

Mouse testes and epididymal sperm were fixed in 3% glutaraldehyde/1% paraformaldehyde/0.1 M sodium cacodylate, pH 7.4 at 4°C overnight and processed for electron microscopy as reported [27]. Images were taken with a Jeol JEM-1230 transmission electron microscope.

Scanning electron microscopy

Mouse epididymal sperm were collected and fixed in the same fixative solution as transmission electron microscopy (TEM). The samples were processed by standard methods [27]. Images were taken with a Zeiss EVO 50 XVP scanning electron microscopy (SEM) at Microscopy Facility, Department of Anatomy and Neurobiology, Virginia Commonwealth University.

Statistical analysis

Analysis of variance (ANOVA) test was used to determine statistical difference; the 2-tailed student's *t*-test was used for comparison of frequencies. Significance is defined as $P < 0.05$.

Results

IFT25 is highly expressed in the mouse testis

To compare *Ift25* mRNA expression levels in mouse tissues, qPCR was conducted using the cDNAs from eight mouse tissues, including heart, brain, spleen, lung, liver, kidney, muscle, and testis. *Ift25* mRNA was highly expressed in the testis (Figure 1A). IFT25 protein expression was examined by western blot analysis. IFT25 protein was detected only in the testis when less sensitive Pico system was used to visualize the protein (Figure 1B). However, when the more sensitive Femto system was used, it was found that IFT25 is also expressed at low level in all the somatic tissues examined (Supplemental Figure 1A). Dynamic expression of IFT25 during the first wave of spermatogenesis was further examined. The protein was detected from day 12 after birth, its expression level appeared to be upregulated from day 24 after birth, when the germ cells enter spermiogenesis, the final phase of spermatogenesis (Figure 1C),

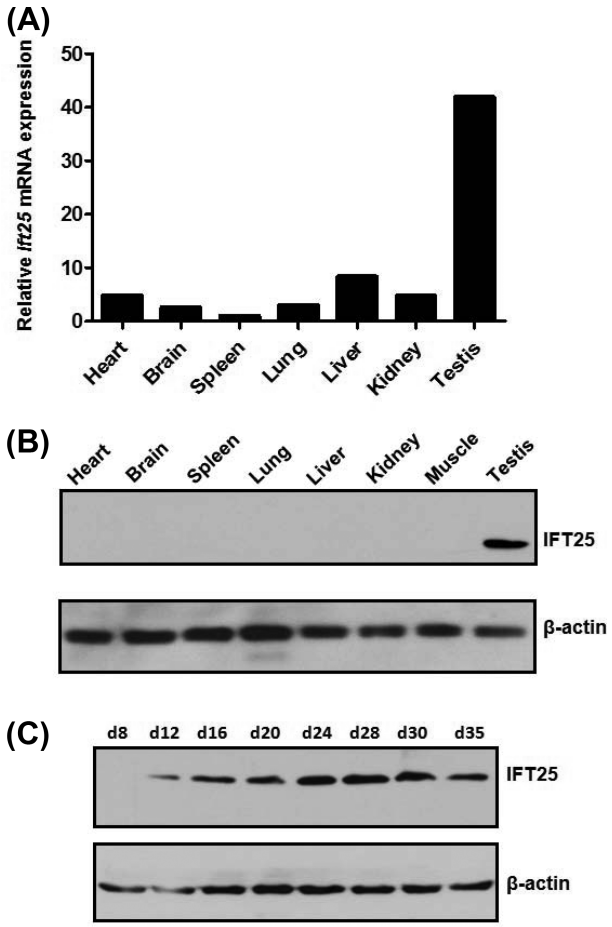

Figure 1. IFT25 is highly expressed in the testis and the protein is upregulated during spermiogenesis. (A) Analysis of relative *Ift25* mRNA expression in adult mouse tissues by qPCR. *Ift25* mRNA expression levels were normalized by *Gapdh*. (B) IFT25 protein expression in adult mouse tissues. Notice that IFT25 was detected only in the testis when less-sensitive Pico system was used. (C) Testicular IFT25 expression during the first wave of spermatogenesis. Notice that the protein was expressed from day 12, when germ cells enter meiosis phase. It appears to be upregulated from day 24, when germ cells enter the final phase, spermiogenesis.

indicating that it plays particular roles in the late stage of spermatogenesis.

Generation of conditional *Ift25* knockout mice

To investigate the role of IFT25 in male germ cell development, the same strategy used to study IFT20 [22] was applied to generate the conditional *Ift25* KO mice. During the whole breeding process, no animal died, and no animal showed any gross abnormalities. The PCR-based genotyping confirmed that homozygous KO mice were obtained (Supplemental Figure 1Ba). Western blot analysis showed that IFT25 protein was completely missing in the testes of the conditional KO mice (Supplemental Figure 1Bb). In the following studies, the *Stra8-icre;Ift25*$^{flox/flox}$ mice were used as KO, and the *Stra8-icre;Ift25*$^{flox/+}$ mice were used as the control.

Conditional *Ift25* KO males are completely infertile

To examine the role of IFT25 in male fertility, KO and control males (6 weeks old or 3–4 months old) were bred to adult wild-type females over a period of 3 months. All the males showed normal mating behavior. However, all KO males at the two age groups were completely infertile, all the control males showed normal fertility (Table 2).

Abnormal sperm in the conditional *Ift25* KO mice

To investigate the mechanisms underlining the infertility phenotype, we first examined cauda epididymal sperm by light microscopy. Sperm collected from the control mice demonstrated normal morphology (Figure 2Aa) and sperm counts (Figure 2B), and had normal motility (Figure 2C and D; Supplemental Figure 2; Supplemental Movies A and C). In contrast, sperm from the *Ift25* KO mice showed multiple morphologic abnormalities, including round heads and tails that were short, bent, or branched. Some spermatozoa had relatively longer tails, but the tail thickness was not even, and some sperm tails appeared to have vacuoles. Some sperm had an abnormal light density along the flagella and some had enlarged tail tips (Figure 2Ab–d; Supplemental Figure 3A). Sperm counts were significantly lower than the controls (Figure 2B). In all mutant mice examined, sperm motility was completely absent (Figure 2C and D; Supplemental Figure 2; Supplemental Movies B and D).

To gain more insight into the abnormal sperm morphology observed under light microscopy, epididymal sperm were further examined by SEM. Sperm from control mice had long and smooth flagella (Figure 3a), but in KO mice normal-appearing flagella were never seen. Instead, all the abnormalities observed in the KO mice under light microscopy were better illustrated by SEM (Figure 3b–f; Supplemental Figure 3B), including short and bent tails (Figure 3b; Supplemental Figure 3Ba and b), round and other misshaped heads (Figure 3c–f; Supplemental 3Bb and c), swollen tail tips (Figure 3d; Supplemental 3Bb–d), and branched tails (Figure 3f). The thickness of numerous sperm flagella was uneven (Figure 3c–e; Supplemental Figure 3Bb and c), and vesicles could be observed in some regions of the flagella (Figure 3c).

Severe spermatogenesis defect in the conditional *Ift25* KO mice

Significantly reduced sperm counts and abnormal sperm morphology strongly suggested a spermatogenesis defect, which led us to examine testicular histology in control and the conditional KO mice. Testis size of the KO mice appeared to be normal, and there was no significant difference in testis and body weights, and testis/body weight ratio (Supplemental Figure 4). In control mice, spermatogenesis was

Table 2. Fertility, fecundity of control and conditional *Ift25* mutant mice.

	Six-weeks-old mice			Adult mice	
Genotype	Fertility	Litter size	Genotype	Fertility	Litter size
Control	10/10	7.8 ± 1.5	Control	10/10	8.1 ± 2.9
Ift25 KO	0/10	0	*Ift25* KO	0/10	0

To test fertility, adult mature and 6-weeks-old males were bred to wild-type females for at least 3 months. Litter size was recorded for each mating.

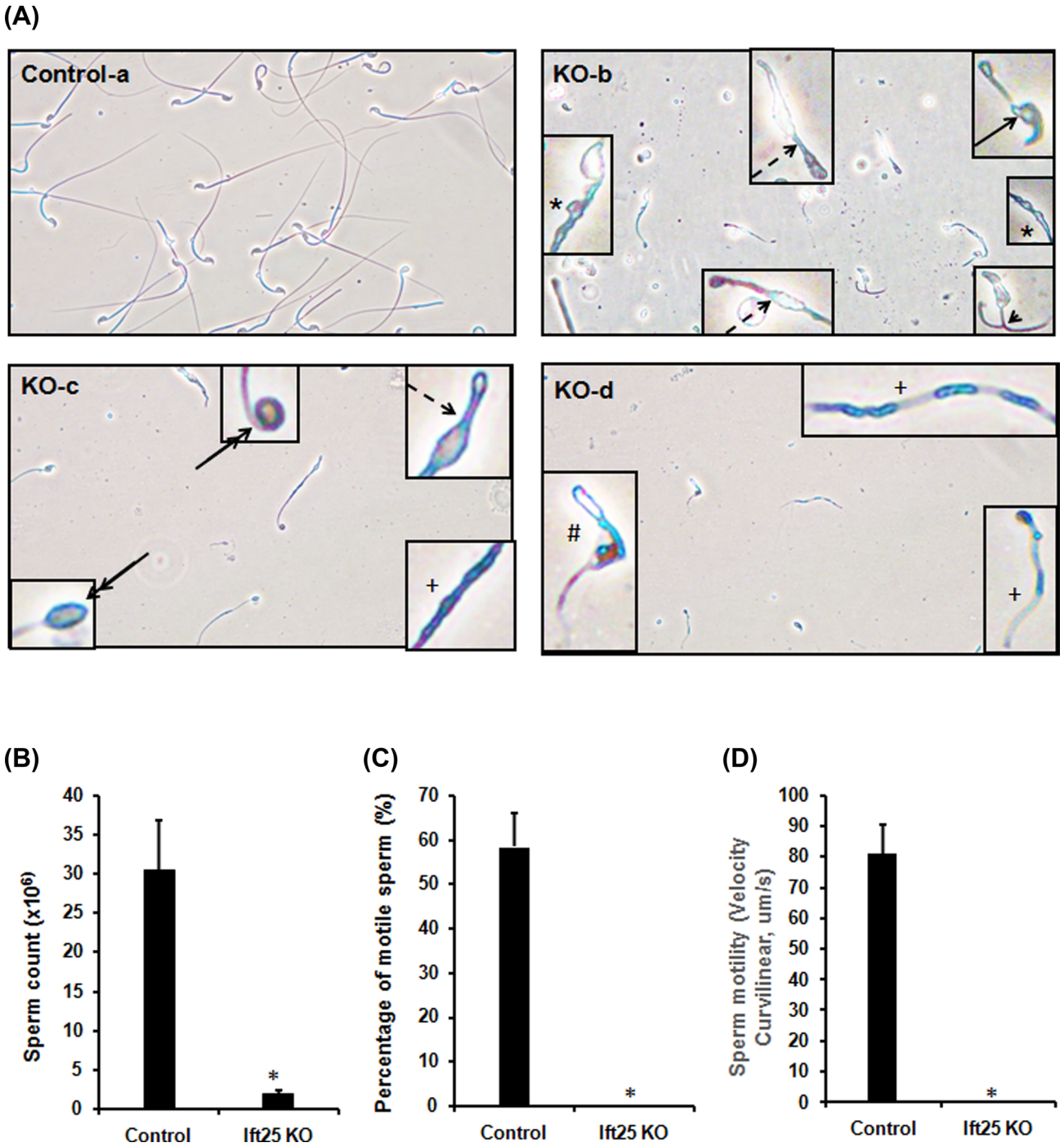

Figure 2. Disruption of *Ift25* gene in germ cells leads to abnormal sperm morphology associated with significantly reduced sperm count and sperm immobility. (A) Examination of epididymal sperm from 3–4-month-old control (a) and conditional *Ift25* KO mice (b–d) by light microscopy. Notice that under the same dilution, compared to the control, much cell debris was present, and very few sperm were seen in the conditional *Ift25* KO mice. Sperm from the KO mice usually had shorter (black arrow in b) or branched tails (black arrowhead in b). Some sperm had longer tails than the others, but vacuoles were present along the tails (dashed arrows in b and c). Double-arrow lines point to the sperm with swollen tails; the asterisk showed the sperm flagella with different thickness; the plus indicated the sperm flagella with different light density, probably stuck IFT particles inside the developing tails; the hash indicates a spermatozoon with a bent tail. (B) Sperm count is significantly reduced in the KO mice. (C and D). Sperm motile in 3–4-month-old control and the KO mice analyzed in PBS. Notice that no sperm showed motility in the KO mice.

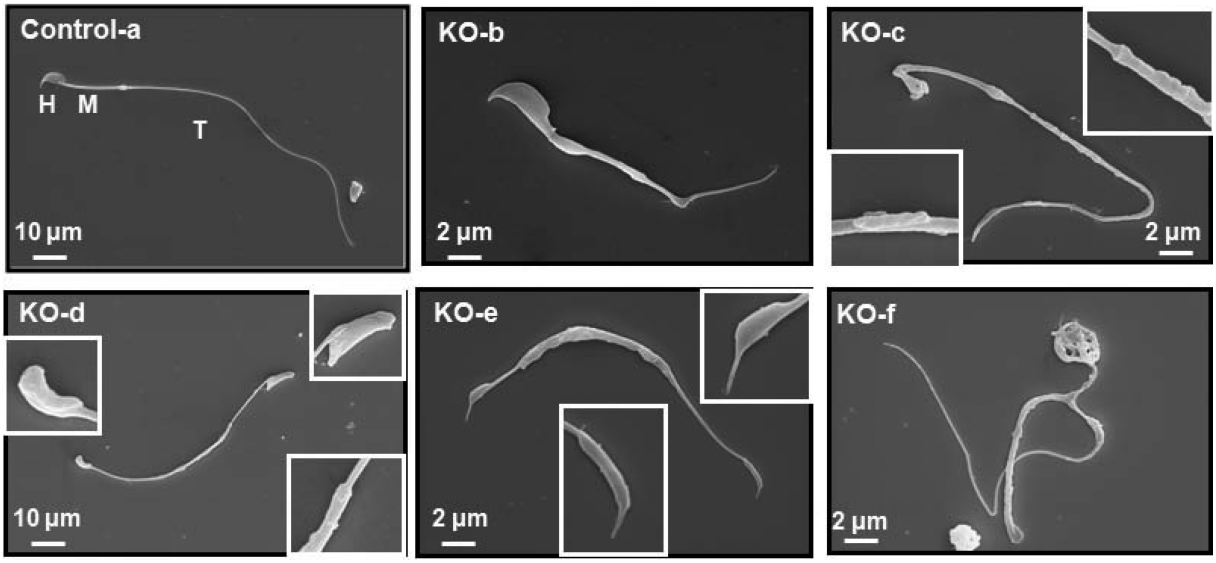

Figure 3. Examination of epididymal sperm by SEM. (a) Representative image of epididymis sperm from a 4-month-old control mouse with normal morphology. The sperm has normally developed midpiece (M), a long and smooth tail (T), and nicely condensed head (H). (b–f) Representative images of epididymal sperm from a 4-month-old KO mouse. Variety of abnormal morphology of sperm from the KO mice was present. Some have short and kinked tails (b), some have round (c), and other misshaped heads (upper right inserts in d and e); some have relatively longer but uneven tails (the two inserts in c, low right insert in d); some have abnormal tail tips (left insert in d, and low insert in e). Some sperm have branched tails (f).

normal, with step 16 spermatids lining the lumen of the seminiferous tubules, with their long tails extending parallel with each other into the lumen. Residual bodies of left over cytoplasm were forming between the sperm heads and the step 7–8 round spermatids (Figure 4A in panel A; Figure 4A–E in panel B). However, in the KO mice, even though mitosis and meiosis phases appeared to be normal, failure of spermatogenesis was observed in the final phase, spermiogenesis (Figure 4B–F in panel A; Figure 4 F–J in panel B), which resulted in fewer sperm in the lumen, abnormal tail, and head formation, with abnormalities in nuclear shape from the step 16 spermatids. There was also failure of spermiation.

Abnormal spermiogenesis was also detected in histological evaluations of the cauda epididymis. In the control mice, the cauda epididymis contained well-developed spermatozoa (Figure 4, panel C). However, in the *Ift25* KO cauda epididymis the lumen was filled with sperm having abnormal misshaped heads and abnormal cytoplasm attached to sperm tails, sloughed spermatids, numerous detached sperm heads and abnormal tails (Figure 4, panel C).

Ultrastructural changes in the epididymal and testicular sperm of the conditional *Ift25* KO mice

To examine ultrastructure changes of sperm in the absence of IFT25, TEM was conducted on the epididymal and testicular sperm of the control and the *Ift25* KO mice. Control mice had normal epididymal sperm ultrastructure. The sperm showed typical "9+2" motile cilia axoneme structure, and accessory structures were present in their correct positions (Figure 5a and b). However, multiple abnormalities were discovered in almost all epididymal sperm recovered from the KO mice, including deformed chromatin, disrupted "9+2" core axoneme structure, disorganized axoneme microtubule array, distorted membranes, misplaced and missing ODFs, and FS (Figure 5c–h).

To understand if these abnormalities were caused during the transporting process from the testis or testis in situ, ultrastructure of testicular sperm was examined by TEM. In the control testis, well-developed sperm were present in the lumen of seminiferous tubules, as indicated by the cross-section of normal axonemes (Figure 6a and b). In the KO testes, flagellar axonemes were rarely seen in seminiferous tubules and lumen (Figure 6c). In the few sperm discovered, none of them showed normal structure, and all displayed the abnormalities as observed in the epididymal sperm, including disrupted "9+2" motile cilia structure, particularly missing central apparatus, misplaced and missing ODFs (outer dense fibers), distorted membranes, and vacuoles in the sperm flagella (Figure 6d–j), indicating that the abnormal ultrastructure observed in the epididymal sperm occurred within the testis.

Mouse IFT25 directly interacts with mouse IFT27

It has been shown that human IFT25 interacts with human IFT27 [12], and *Chlamydomonas* IFT25 also interacts with *Chlamydomonas* IFT27 [17]. To determine if this interaction is a universal phenomenon among all species, we examined the interaction in the mouse by direct yeast two-hybrid assay. Like the positive control, yeast transformed with the IFT25/IFT27 pair grew on both selection and nonselection plates (Supplemental Figure 5A), indicating that mouse IFT25 does interact with mouse IFT27 in yeast. To further examine if mouse IFT25 and IFT27 interact in vivo, co-IP was conducted using mouse testicular extract. When the anti-IFT27 antibody was used to pull-down the protein complex, not only was IFT27 precipitated, IFT25 was also coprecipitated (Supplemental Figure 5B).

IFT25 regulates expression levels of other intraflagellar transport proteins, particularly IFT27 in male germ cells.

IFT proteins usually form a complex with other IFT proteins. To explore the potential functional relationship between IFT25 and other IFT proteins, levels of selective IFT proteins in the testis were examined by western blot analysis in the control and the *Ift25* KO mice (Figure 7A). IFT27, the IFT25-binding partner was completely

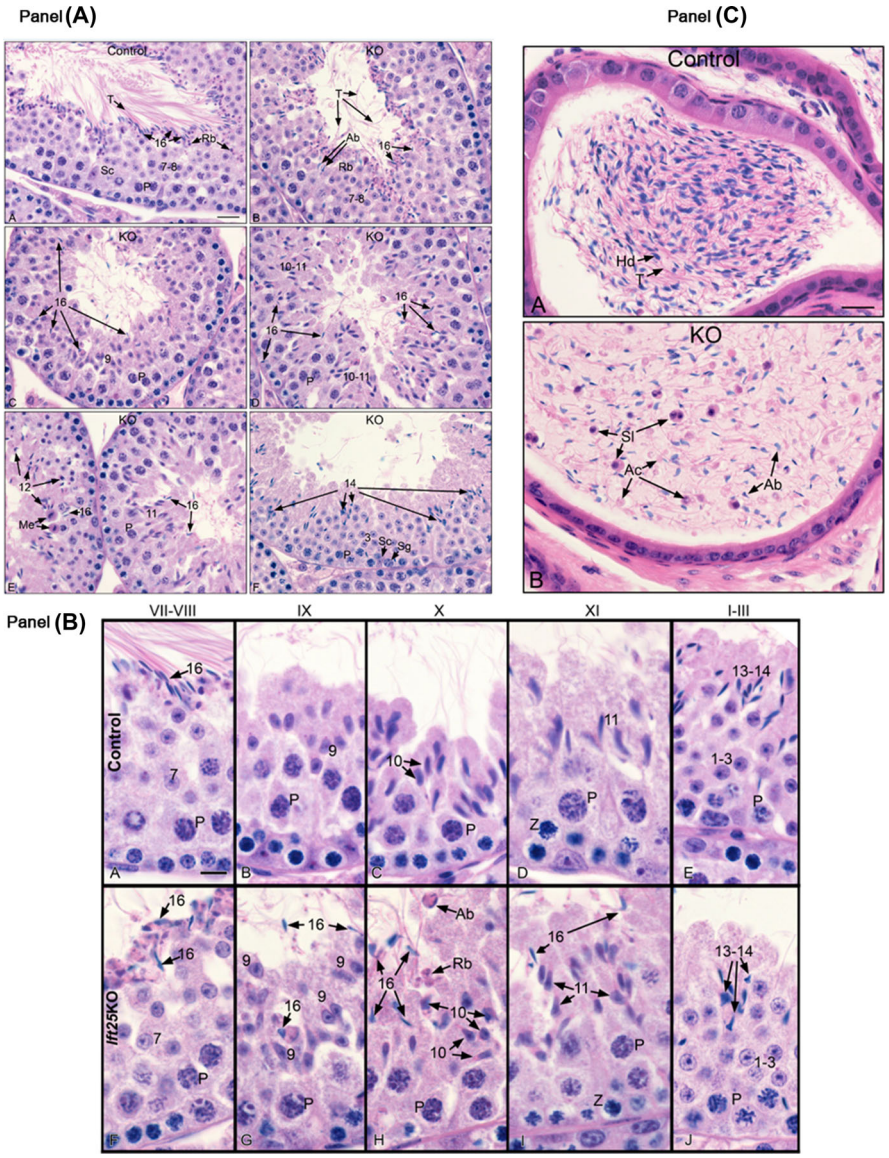

Figure 4. Testicular and epididymal histology of adult control and *Ift25* KO mice. Panel A: (A) control testis showing stage VII-VIII. Step 16 spermatids line the lumen, with their long tails (T) extending parallel into the lumen. Residual bodies (Rb) of left over cytoplasm are forming between the sperm heads and the step 7–8 round spermatids. Sc, Sertoli cell; P, pachytene spermatocytes. Bar = 20 μm. (B–F) *Ift25* KO mice testes. (B) Stage VII-VIII, showing abnormal tail (T) formation from the step 16 spermatids. Abnormal step 16 spermatid head (Ab) are present above the nuclei of step 7–8 round spermatids. (C) Stage IX, showing failure of spermiation with step 16 spermatid head being retained within the seminiferous epithelium and among the step 9 spermatids that are just beginning to change shape. P, pachytene spermatocytes. (D) Stage X-XI, showing step 16 spermatid head being retained in the epithelium along with step 10–11 spermatids having large variation in shape, with the beginning of abnormal formations. P, pachytene spermatocytes. (E) Stage XII on the left and stage XI on the right. Step 16 spermatid head are seen retained in the epithelium and abnormal step 11–12 spermatids are seen due to alterations in nuclear shape. Me, necrotic spermatocytes in meiotic division. (F) Stage III, showing numerous step 14 elongating spermatid heads. Step 3 round spermatid nuclei are normal in appearance. Sc, Sertoli cell; P, pachytene spermatocyte; Sg, spermatogonium. Panel B. Control (A–E) and *Ift25* KO (F–J). Round spermatids are indicated by 1–7. Elongating spermatids are indicated by 9–16. P, pachytene spermatocyte; Z, zygotene spermatocyte. Bar = 10 μm for all photos. Stage VII-VIII: control and *Ift25* KO step 7 round spermatids are normal. Elongated spermatids step 16 in control have thin, highly condensed nuclei that are aligned at the lumen for spermiation, but in the KO step 16 spermatids show abnormal alignment and head formations. P, pachytene spermatocytes. Bar = 10 μm for all photos. Stage IX: step 9 spermatids in control show the beginning of head elongation. In the *Ift25* KO some step 9 cells are normal, but there is an inconsistent change in spermatid head elongation. There are also step 16 spermatid heads that were not released, an indication of failure of spermiation. Stage X: step 10 spermatids in controls have elongated and show the typical protrusion of the condensing head. However, step 10 spermatid heads in *Ift25* KO males show significant abnormality in shape and appear disorganized in the epithelium. Numerous step 16 spermatids remain attached to the epithelium after failure of spermiation in stage VIII. An abnormal aggregate of step 16 spermatid heads (Ab) is seen near the lumen. Residual bodies (Rb) are also retained abnormally near the lumen. Stage XI: control step 11 elongating spermatids are well formed in the seminiferous epithelium above the large pachytene spermatocytes (P). In *Ift25* KO, step 11 cell nuclei show abnormal shapes, and the heads of step 16 spermatids remain attached, rather than being released into the lumen. Stage I-III: round spermatids (1-3) appear normal in shape and numbers in both control and *Ift25* KO testes. In control, the elongating spermatids steps 13–14 have condensed chromatin heads that are positioned throughout the epithelium. In *Ift25* KO, step 13–14 cells show multiple head abnormal shapes, which appeared first in earlier stages. Panel C: cauda epididymis from control and *Ift*25 KO mice. Control sperm are highly concentrated in the cauda region, showing the head (Hd) and tails (T). In *Ift*25 KO, the cauda epididymis lumen is filled with abnormal sperm heads (Ab), abnormal cytoplasm attached to sperm tails (Ac), sloughed spermatids (Sl), numerous detached sperm heads and abnormal tails.

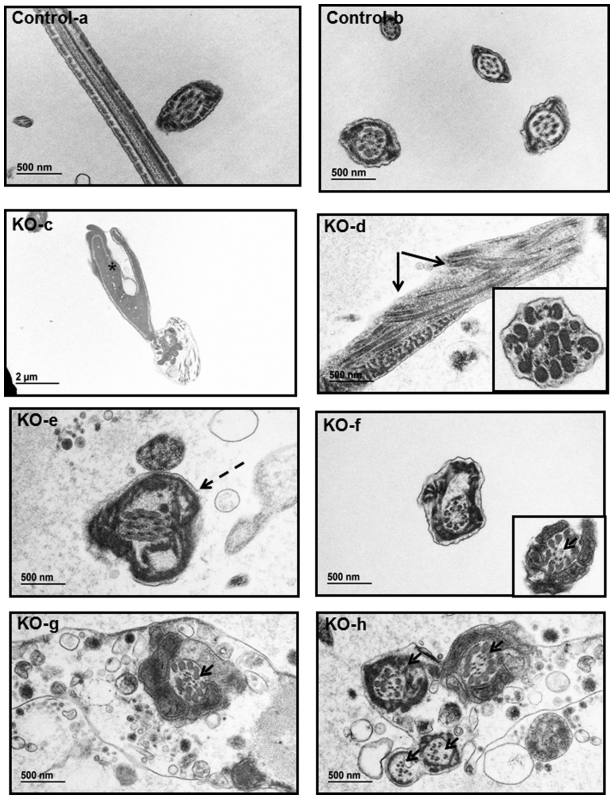

Figure 5. Analysis of epididymal sperm of the control and *Ift25* KO mice by TEM. TEM images of epididymal sperm from 4-month-old control and KO mice. Sperm from the control mice show normal ultrastructure (a, b). However, most sperm from the *Ift25* KO demonstrate multiple abnormalities, including abnormal head (asterisk in c), disorganized microtubule array (arrows in d), distorted membranes (dashed arrow in e); some sperm lose "9+2" core axoneme structure (arrow heads in f, g, h); some have disorganized (insert in d), or missing accessary structures, including ODF and fibrous sheath (g, h).

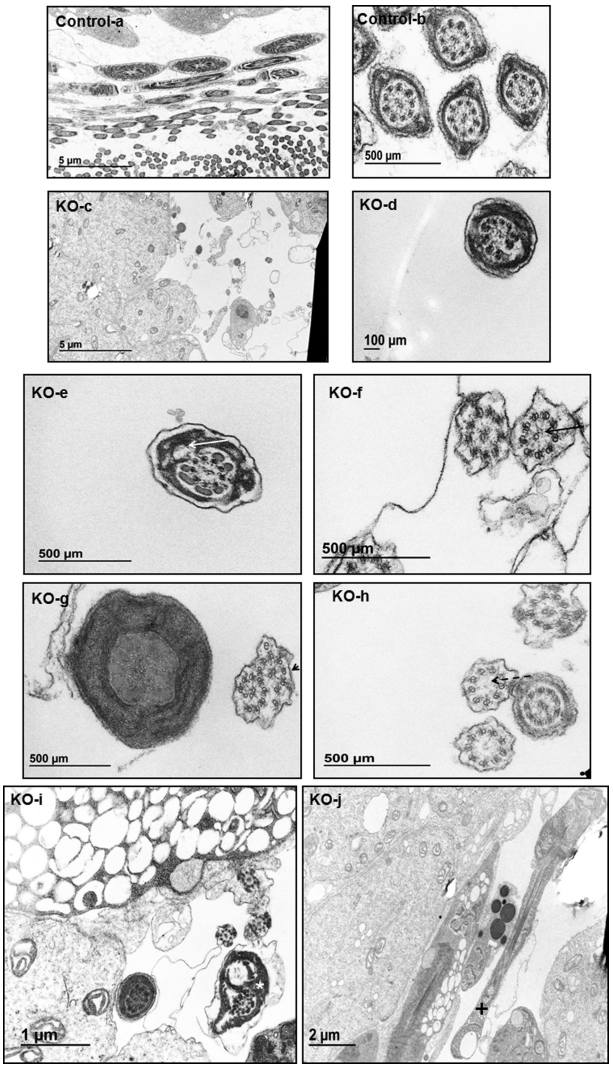

Figure 6. Analysis of testicular sperm of the control and *Ift25* KO mice by TEM. TEM images of testicular sperm from 4-month-old control and KO mice. In the control mice, sperm were easily discovered in the lumen of seminiferous tubules (a), and the ultrastructure was normal (b). However, few sperm were discovered in the KO (c), and the sperm usually have disorganized axoneme structure (d). The white arrow in "e" points to an axoneme missing several ODFs; the black arrow in "f" points to an axoneme missing one of the two central microtubule; the arrow head in "g" points to an axoneme with extra microtubules; the dashed arrow in "h" points to an axoneme missing the entire central microtubules; the white asterisk in "i" shows a sperm with distorted membrane; and the plus in "j" shows a sperm with a vacuole in the tail.

missing in the *Ift25* KO mice, and expression levels of IFT20 and IFT81 were also significantly reduced. However, expression levels of IFT74 and IFT140 were not changed (Figure 7B). Coimmunoprecipitation was conducted to examine if IFT20, IFT81, and IFT25 were in the same complex in vivo. An anti-IFT25 antibody was used to pull down testicular extract, and the presence of IFT20 and IFT81 proteins was examined by specific antibodies. Both IFT20 and IFT81, components of IFT-B complex, were coprecipitated (Figure 7C).

Discussion

The present study reveals the phenotype of mouse *Ift25* gene inactivation in male germ cells, and compares protein expression levels of several other selected IFT proteins between the control and conditional IFT25 KO mice. We discovered that KO male infertility was associated with severe defects in the final phase of spermatogenesis, spermiogenesis. Only a few germ cells were capable of completing spermatogenesis and forming spermatozoa. However, those developed sperm lost complete motility and displayed abnormal flagella structure, particularly the accessory structures and most also had abnormal heads.

This severe phenotype was unexpected. As noted, genes encoding IFT25 homologs are absent from the genomes of organisms that lack cilia and flagella and also from those of *Drosophila melanogaster* and *Caenorhabditis elegans*, indicating that IFT25 has a specialized role in IFT that is not required for the assembly of cilia or flagella in the worm and fly [12], and this is also supported by the observations from the mouse model that *Ift25* was disrupted ubiquitously. Straight knockout of *Ift25* resulted in multiple phenotypes related to the disruption of Hedgehog signaling pathway localized in the primary cilia; however, ciliogenesis was not affected as demonstrated by normal cilia morphology in MEFs, tracheal epithelial cells, and hair cells [19, 20]. Apparently, IFT25 plays different roles in the development of cilia/flagella in somatic cells and male germ cells. In the present model, *Ift25* was inactivated only in germ cells. As expected, all KO mice survived to adulthood and did not show any gross

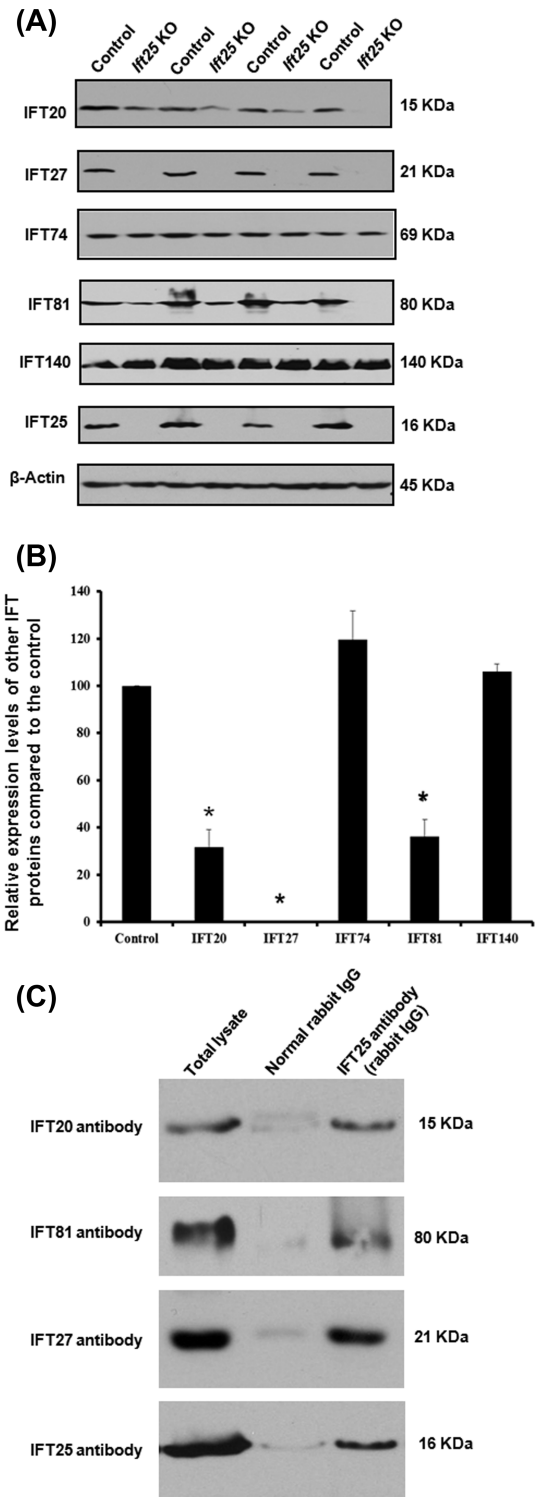

Figure 7. Regulation of other IFT proteins in absence of IFT25 in male germ cells. (A) Representative western blot results using the indicated IFT antibodies. Notice that IFT27, the IFT25 binding partner, is missing in the testes of the *Ift25* KO mice. Testicular expression of IFT20 and IFT81 were also reduced in the KO. (B) Statistical analysis of relative expression of the IFT proteins normalized by β-actin. There is no difference in expression levels of IFT74 and IFT140 between the controls and the *Ift25* KO mice. IFT20 and IFT81 expression levels are significantly reduced in the KO. (C) Both IFT20 and IFT81 are present in the IFT25 complex in mouse testis. Testicular extract was pulled down with anti-IFT25 antibody, and western blottings were conducted using anti-IFT25, anti-IFT20, and anti-IFT81 antibodies.

abnormalities during the whole developmental stage. However, all KO males were infertile, presumably due to both significantly reduced sperm counts and disrupted development of the sperm head/flagella structures. All sperm, including those with short tails, and those with relatively long tails, showed no motility. Under light microscopy and SEM, a striking observation was sperm with branched flagella, and flagella that had variable thicknesses along the lengths of their tails, and the occasional swollen tail tips. TEM also showed vesicles/vacuoles in some area along the flagella. It is likely that the IFT mechanism is disrupted in the germ cells lacking IFT25, and cargo vesicles are not being transported efficiently and incorporated in the flagellum. A typical phenotype for ciliary retrograde transport failure is to form a bulb at the ciliary tip [28, 29]. Even though IFT25 is considered to be an IFT-B component, and disruption of IFT-B genes usually results in short cilia/flagella [28–30], the swollen tail tips in the IFT25-deficient mice suggested that IFT25 might also be involved in retrograde transport. This is supported by SEM studies that showed irregularities all along some of the tails, and perhaps the accumulation at the end could be failure of vesicles to attach to the appropriate destination, causing them to accumulate at the end.

The mechanism(s) involving IFT25 regulation of spermatogenesis, sperm motility, and flagella integrity are not clear. IFT25 is present as a complex with other IFT-B proteins [10, 17]. In order to explore the possibility that the phenotype is due to altered expression of other IFT proteins in the absence of IFT25, expression levels of selected IFT protein, including IFT-B complex components, IFT20, IFT27, IFT74, IFT81, and IFT-A complex component, IFT140 were examined [31–39]. Not surprisingly, IFT140, as well as IFT74 expression levels were not changed. However, IFT27, an IFT25-binding partner, was missing in the KO mice. IFT20 and IFT81 expression levels were also significantly reduced. Similar to *Ift25* gene, *Ift27* is another gene absent from the genomes of organisms that lack cilia and flagella and also from those of *Drosophila melanogaster* and *Caenorhabditis elegans*. We also disrupted mouse *Ift27* gene in mouse germ cells, and the phenotype was similar to the present *Ift25* KO model, although there appeared to be several important differences (unpublished observation).

IFT20 is another IFT-B complex component. Our laboratory also disrupted this gene in male germ cells. Similar to the *Ift25* KO mice, conditional *Ift20* KO adult males were infertile with a defect in sperm flagella assembly [22]. However, some IFT20-deficient germ cells retained redundant cytoplasm, which was not observed in the conditional *Ift25* KO mice. Some sperm were still motile in the *Ift20* KO mice, even though the motility was significantly reduced [22]. However, no sperm were motile in the *Ift25* KO mice. Thus, it is unlikely that IFT20 and IFT25 function in exactly the same mechanism. Both are involved in flagella assembly, probably through IFT mechanisms, but they have their unique roles in modeling sperm flagella structure and motility. The downregulation of IFT20 and IFT81 in the *Ift25* KO might be the result of fewer germ cells having been enriched with these two proteins in the IFT25-deficient mice. It is also possible that these IFT proteins are in the same complex in male germ cells, and IFT25 stabilizes IFT20 and IFT81. Without IFT25, IFT20 and IFT81 are less stable. Our co-IP experiment confirmed that IFT25, IFT20, and IFT81 are indeed in the same complex. The role of IFT81 in male germ cell development remains to be determined.

The absence of flagella motility of the *Ift25* KO mice is fascinating. In addition to normal structure [40–43], other factors also contribute to normal sperm motility, including the

calcium (Ca2+) pathway and the cyclic adenosine monophosphate (cAMP)-dependent protein kinase or protein kinase A pathways, ion channels, reactive oxygen species (ROS), and control of cell volume and osmolarity [44–69]. IFT25 contains a galactose-binding like domain (IPR008979), which in other proteins binds various ligands such as carbohydrates, phospholipids, and nucleic acids [69, 70]. It has been shown that overexpression of IFT25/Hsp16.2 activates Hsp90, and stabilizes lipid rafts by the activation of PI-3-kinase-Akt cytoprotective pathway [14]. Lipid rafts are specialized membrane microdomains that function as signaling platforms across plasma membranes of many animal and plant cells [71, 72] and have been identified in sperm [73, 74]. Recent studies suggest that sperm lipid rafts function in signaling upstream of cAMP synthesis, and are required for Ca(2+)-dependent pathways underlying activation in *Ciona* sperm [75]. Because it has been shown that IFT is required for some ion channels to be localized to the cilium [76, 77], it is possible that IFT25 complex is also responsible for carrying certain ion channels to the sperm flagellum. It remains to be determined if lipid rafts and calcium signal are altered in the *Ift25* KO sperm.

TEM studies revealed that some *Ift25* KO sperm lost microtubules of the central apparatus, a structure only present in the motile cilia [78]. The central apparatus has been shown to be a key structure to regulate ciliary/flagellary motility; thus, the missing central apparatus likely contributes significantly to immotility of the *Ift25* KO sperm [79]. Another interesting finding in the conditional *Ift25* KO mice was the disruption in FS formation. The FS is a unique cytoskeletal structure surrounding the axoneme and outer dense fibers. It consists of two longitudinal columns connected by closely arrayed circumferential ribs that assemble from distal to proximal throughout spermiogenesis [80]. The FS functions as a scaffold for proteins in signaling pathways that might be involved in regulating sperm maturation, motility, capacitation, hyperactivation, and/or acrosome reaction and for enzymes in the glycolytic pathway that provide energy for the hyperactivated motility of sperm [81, 82]. Given that the FS is only present in the sperm flagella and not in other cilia/flagella, and the fact that IFT25 is not required for ciliogenesis for other cilia/flagella [19, 20], it is highly possible that IFT25 plays its unique role in sperm flagella formation by remodeling the FS during spermiogenesis.

In the transfected mammalian cells, IFT25 was localized to the centrioles and cilia, the typical localizations of IFT proteins [10]. Because IFT25 plays a unique function in male germ cells, it apparently forms a unique complex in these nonsomatic cells, and to fulfill its function it may also require this unique localization. Unfortunately, because we had no success with immunofluorescence staining of male germ cells using three IFT25 antibodies that worked for western blot analysis, we do not know its specific localization. Thus far, IFT27 is the only protein that has been confirmed to interact with IFT25. Therefore, identification of the components of the IFT25 complex in male germ cells will also be necessary to understand its unique role in male germ cell development. These studies are currently being conducted in our laboratory.

In the present study, we analyzed ultrastructural changes of epididymal and testicular sperm; however, we do not know when these abnormalities occur during germ cell development. To answer this question, a close observation of the ultrastructure of germ cells at each step is needed. Particularly, IFT25 has been reported to be localized in the basal body in somatic cells [10]. Defects in this structure in the elongating spermatids should be paid additional attention because basal bodies are the template of the developing flagella [83]. From our present findings, we deduced that mitosis and meiosis phases appear to be normal. However, abnormalities occur in spermiogenesis when germ cells start changing morphology, including flagella formation. Even though we do not know where IFT25 localizes in male germ cells, we assume the locations should be related to the cargo transport system in the elongating spermatids, including the manchette and the developing axoneme. The manchette is a unique structure only present in the elongating spermatids [84]. Its proposed function is to transport cargo proteins to the basal bodies for sperm flagella formation [85]. IFT20 is localized in this structure [86]. Given that IFT20 and IFT25 are in the same complex, it is possible that IFT25 is also present in the manchette and plays a role in transporting cargo proteins along the manchette in addition to its role in the developing axoneme. Axoneme defects observed in this model might also be caused by the direct role of IFT25 in assembling the sperm axoneme. Recent studies demonstrated that abnormal accessory structure formation might cause axoneme defects [87]. It is also possible that the core axoneme defect in the *Ift25* KO sperm was caused partially by the accessory defects.

Abnormal spermiation observed in the conditional *Ift25* KO mice may also contribute to the reduced sperm number. Spermiation is the process of releasing sperm into the lumen from the seminiferous epithelium [88]. A similar phenotype was also observed in the conditional *Ift20* KO mice [40]; thus, IFT25 and IFT20 might coordinate to regulate spermiation.

The database, Esembl, reported five mouse *Ift25* transcripts, Hspb11-001 to Hspb11-005. Hspb11-002 and Hspb11-005 do not translate any protein, and the other three transcripts have different 5′ or 3′ UTRs, but translate the same protein. Our RT-PCR, using the primer set encompassing the full length of the coding region, amplified only one amplicon from mouse testis cDNA, suggesting that only one IFT25 protein was in mouse testis. Western blotting using three different anti-IFT25 antibodies also revealed only one full length IFT25 protein in mouse testis, and the protein was completely missing in the testes of the conditional *Ift25* KO mice. It is unlikely the phenotype was from disruption of another *Ift25* isoform.

Overall, we studied the role of IFT25 in male germ cells, and discovered that even though this protein is dispensable for cilia formation of primary cilia and motile cilia of tracheal epithelial cells, it is indispensable for sperm flagella formation and sperm motility. This study uncovers a unique role of IFT25 in germ cell development. IFT25 might conduct multiple functions in germ cells' development and flagella formation, but the mechanisms need further investigation.

Supplementary data

Supplementary data are available at *BIOLRE* online.

Supplemental movies. Examples of sperm motility patterns from the conditional *Ift25* KO and the control mice. Presented in the movies are short segments of freshly isolated, non-capacitated sperm from the control (A and C) and the conditional *Ift25* KO mice. (B and D). Sperm were in PBS in movies A and B; in a non-capacitation medium in movies C and D. All segments were captured with a DAGE-MTI DC-330 3CCD camera and a Canon Optura 40 digital camcorder. Segments were assembled into the video using iMovie HD on a Dual 1GHz 414 PowerPC Processor G4 Apple Macintosh computer.
Movie A and C. Representative movies from control mice. Notice that most sperm are motile and display vigorous flagellar activity and progressive long track forward movement.

Movie B and D. Representative movies from conditional *Ift25* KO mice. Notice that there are less sperm compared to the control mice in the same dilution, and no sperm are motile at all.

Supplementary Figure S1. IFT25 expression in the wild-type and *Ift25* KO mice.

A. IFT25 expression in mouse tissues examined with highly sensitive Pico system. Notice that besides in the testis, IFT25 protein is also expressed in all the somatic tissues examined.

B. IFT25 is absent from the testes of conditional *Ift25* KO mice.

a. Representative genotyping result using specific primers for PCR. Upper panel: primer set to analyze *Ift25* genotyping; Lower panel: primer set to detect Cre.

b. Examination of testicular IFT25 protein expression by Western blot using Pico system. Notice that IFT25 was expressed in the three control mice. However, no specific signal was observed in the three KO mice analyzed.

Supplementary Figure S2. Sperm motility analyzed in a non-capacitation medium. Sperm were collected into a non-capacitation medium from cauda epididymides of 4-month old control and conditional *Ift25* KO mice. Ten minutes after collection, sperm were analyzed for motility. Three control and three KO mice were analyzed.

Supplementary Figure S3. More images showing abnormal sperm from the conditional *Ift25* KO mice.

A. Images taken by light microscopy (a-f). The two inserts in "a" show vesicles in the tail; the inserts in "b" show sperm flagella with different thickness (black arrow), different light density (dashed arrow), and swollen tail tip (arrow head); the inserts in "c" show sperm with swollen tail tips (arrow heads), flagella with different light density (black arrow), and round head (*); the insert in "d" shows a flagellum with uneven thickness along the tail; the inserts in "e" show a spermatozoa with short tail and swollen tail tip (black arrow), a spermatozoa with short tail, swollen tail tip, and round head (dashed arrow), and a sperm flagella with multiple vesicles (arrow head); the inserts in "f" show a spermatozoa with short tail and swollen head and tail tip (black arrow), and a spermatozoa with a bent tail (dashed arrow).

B. Images taken by SEM. Sperm with bent and coiled tail (a); round heads (b, c) and uneven tail thickness (b, c, d); swollen tail tips (b, c).

Supplementary Figure S4. Body weight and testis weight of control and conditional *Ift25* KO mice. Notice that there are no differences in body weight, testis weight and testis weight/body weight between the control and conditional *Ift25* KO mice.

Supplementary Figure S5. Mouse IFT25 interacts with mouse IFT27.

A. Direct yeast two-hybrid assay. The competent AH109 yeast was transformed with the indicated plasmids. Like the positive p53/Large T antigen pair, yeast transformed with IFT25/IFT27 pairs grew on the plates with both non-selection (upper panel) and selection (lower panel) medium, indicating that mouse IFT25 interacts with mouse IFT27.

B. Co-immunoprecipitation assay. Mouse testicular extract was pulled down using an anti-IFT27 antibody, and Western blot was conducted using an anti-IFt27 antibody and an anti-IFT25 antibody. IFT25 was co-precipitated together with IFT27 by the anti-IFT27 antibody.

Acknowledgments

We thank Dr. Scott C. Henderson and Judy C. Williamson for their assistance with using the electronic microscopy in Microscopy Core Facility of Virginia Commonwealth University.

Authors' contributions: Zhibing Zhang designed the experiments and wrote the paper. HL, WL, YZ, Zhengang Zhang, XS, LZ, YL, SZ, AVS, BD, and Zhibing Zhang performed the experiments. GLG and GJP contributed reagents and materials. JAF, RAH, and Zhibing Zhang analyzed the data.

Conflict of Interest: The authors have no conflict of interest.

References

1. Malicki JJ, Johnson CA. The Cilium: cellular antenna and central processing unit. *Trends Cell Biol* 2017; **27**:126–140.
2. Rohatgi R, Snell WJ. The ciliary membrane. *Curr Opin Cell Biol* 2010; **22**:541–546.
3. Emmer BT, Maric D, Engman DM. Molecular mechanisms of protein and lipid targeting to ciliary membranes. *J Cell Sci* 2010; **123**:529–536.
4. Pedersen LB, Mogensen JB, Christensen ST. Endocytic control of cellular signaling at the primary cilium. *Trends Biochem Sci* 2016; **41**:784–797.
5. Prasad RM, Jin X, Nauli SM. Sensing a sensor: identifying the mechanosensory function of primary cilia. *Biosensors (Basel)* 2014; **4**:47–62.
6. Kozminski KG, Johnson KA, Forscher P, Rosenbaum JL. A motility in the eukaryotic flagellum unrelated to flagellar beating. *Proc Natl Acad Sci USA* 1993; **90**:5519–5523.
7. Rosenbaum JL, Witman GB. Intraflagellar transport. *Nat Rev Mol Cell Biol* 2002; **3**:813–825.
8. Taschner M, Lorentzen E. The intraflagellar transport machinery. *Cold Spring Harb Perspect Biol* 2016; **8**:a028092.
9. Pedersen LB, Rosenbaum JL. Intraflagellar transport (IFT) role in ciliary assembly, resorption and signalling. *Curr Top Dev Biol* 2008; **85**:23–61.
10. Follit JA, Xu F, Keady BT, Pazour GJ. Characterization of mouse IFT complex B. *Cell Motil Cytoskeleton* 2009; **66**:457–468.
11. Pazour GJ, Agrin N, Leszyk J, Witman GB. Proteomic analysis of a eukaryotic cilium. *J Cell Biol* 2005; **170**:103–113.
12. Rual JF, Venkatesan K, Hao T, Hirozane-Kishikawa T, Dricot A, Li N, Berriz GF, Gibbons FD, Dreze M, Ayivi-Guedehoussou N, Klitgord N, Simon C et al. Towards a proteome-scale map of the human protein-protein interaction network. *Nature* 2005; **437**:1173–1178.
13. Bohn H, Winckler W. Isolation and characterization of five new soluble placental tissue proteins (PP22, PP23, PP24, PP25, PP26). *Arch Gynecol Obstet* 1991; **248**:111–115.
14. Bellyei S, Szigeti A, Boronkai A, Pozsgai E, Gomori E, Melegh B, Janaky T, Bognar Z, Hocsak E, Sumegi B, Gallyas F, Jr. Inhibition of cell death by a novel 16.2 kD heat shock protein predominantly via Hsp90 mediated lipid rafts stabilization and Akt activation pathway. *Apoptosis* 2007; **12**:97–112.
15. Bellyei S, Szigeti A, Pozsgai E, Boronkai A, Gomori E, Hocsak E, Farkas R, Sumegi B, Gallyas F, Jr. Preventing apoptotic cell death by a novel small heat shock protein. *Eur J Cell Biol* 2007; **86**:161–171.
16. Lechtreck KF, Luro S, Awata J, Witman GB. HA-tagging of putative flagellar proteins in Chlamydomonas reinhardtii identifies a novel protein of intraflagellar transport complex B. *Cell Motil Cytoskeleton* 2009; **66**:469–482.
17. Wang Z, Fan ZC, Williamson SM, Qin H. Intraflagellar transport (IFT) protein IFT25 is a phosphoprotein component of IFT complex B and physically interacts with IFT27 in Chlamydomonas. *PLoS One* 2009; **4**:e5384.
18. Bhogaraju S, Taschner M, Morawetz M, Basquin C, Lorentzen E. Crystal structure of the intraflagellar transport complex 25/27. *EMBO J* 2011; **30**:1907–1918.
19. Keady BT, Samtani R, Tobita K, Tsuchya M, San Agustin JT, Follit JA, Jonassen JA, Subramanian R, Lo CW, Pazour GJ. IFT25 links the signal-dependent movement of Hedgehog components to intraflagellar transport. *Dev Cell* 2012; **22**:940–951.
20. Yang N, Li L, Eguether T, Sundberg JP, Pazour GJ, Chen J. Intraflagellar transport 27 is essential for hedgehog signaling but dispensable for ciliogenesis during hair follicle morphogenesis. *Development* 2015; **142**:2194–2202.

21. Sadate-Ngatchou PI, Payne CJ, Dearth AT, Braun RE. Cre recombinase activity specific to postnatal, premeiotic male germ cells in transgenic mice. *Genesis* 2008; **46**:738–742.
22. Zhang Z, Li W, Zhang Y, Zhang L, Teves ME, Liu H, Strauss JF, 3rd Pazour GJ, Foster JA, Hess RA, Zhang Z. Intraflagellar transport protein IFT20 is essential for male fertility and spermiogenesis in mice. *Mol Biol Cell* 2016; **27**:3705–3716.
23. Pazour GJ, Baker SA, Deane JA, Cole DG, Dickert BL, Rosenbaum JL, Witman GB, Besharse JC. The intraflagellar transport protein, IFT88, is essential for vertebrate photoreceptor assembly and maintenance. *J Cell Biol* 2002; **157**:103–113.
24. Jonassen JA, SanAgustin J, Baker SP, Pazour GJ. Disruption of IFT complex A causes cystic kidneys without mitotic spindle misorientation. *J Am Soc Nephrol* 2012; **23**:641–651.
25. Zhang Z, Shen X, Gude DR, Wilkinson BM, Justice MJ, Flickinger CJ, Herr JC, Eddy EM, Strauss JF, 3rd. MEIG1 is essential for spermiogenesis in mice. *Proc Natl Acad Sci USA* 2009; **106**:17055–17060.
26. Navarrete FA, Garcia-Vazquez FA, Alvau A, Escoffier J, Krapf D, Sanchez-Cardenas C, Salicioni AM, Darszon A, Visconti PE. Biphasic role of calcium in mouse sperm capacitation signaling pathways. *J Cell Physiol* 2015; **230**:1758–1769.
27. Zhang Z, Kostetskii I, Tang W, Haig-Ladewig L, Sapiro R, Wei Z, Patel AM, Bennett J, Gerton GL, Moss SB, Radice GL, Strauss JF, 3rd. Deficiency of SPAG16L causes male infertility associated with impaired sperm motility. *Biol Reprod* 2006; **74**:751–759.
28. Pedersen LB, Geimer S, Rosenbaum JL. Dissecting the molecular mechanisms of intraflagellar transport in chlamydomonas. *Curr Biol* 2006; **16**:450–459.
29. Qin H, Diener DR, Geimer S, Cole DG, Rosenbaum JL. Intraflagellar transport (IFT) cargo: IFT transports flagellar precursors to the tip and turnover products to the cell body. *J Cell Biol* 2004; **164**:255–266.
30. Ishikawa H, Marshall WF. Ciliogenesis: building the cell's antenna. *Nat Rev Mol Cell Biol* 2011; **12**:222–234.
31. Lucker BF, Behal RH, Qin H, Siron LC, Taggart WD, Rosenbaum JL, Cole DG. Characterization of the intraflagellar transport complex B core: direct interaction of the IFT81 and IFT74/72 subunits. *J Biol Chem* 2005; **280**:27688–27696.
32. Bhogaraju S, Cajanek L, Fort C, Blisnick T, Weber K, Taschner M, Mizuno N, Lamla S, Bastin P, Nigg EA, Lorentzen E. Molecular basis of tubulin transport within the cilium by IFT74 and IFT81. *Science* 2013; **341**:1009–1012.
33. Brown JM, Cochran DA, Craige B, Kubo T, Witman GB. Assembly of IFT trains at the ciliary base depends on IFT74. *Curr Biol* 2015; **25**:1583–1593.
34. Kubo T, Brown JM, Bellve K, Craige B, Craft JM, Fogarty K, Lechtreck KF, Witman GB. Together, the IFT81 and IFT74 N-termini form the main module for intraflagellar transport of tubulin. *J Cell Sci* 2016; **129**:2106–2119.
35. Duran I, Taylor SP, Zhang W, Martin J, Forlenza KN, Spiro RP, Nickerson DA, Bamshad M, Cohn DH, Krakow D. Destabilization of the IFT-B cilia core complex due to mutations in IFT81 causes a Spectrum of Short-Rib Polydactyly Syndrome. *Sci Rep* 2016; **6**:34232.
36. Fort C, Bonnefoy S, Kohl L, Bastin P. Intraflagellar transport is required for the maintenance of the trypanosome flagellum composition but not its length. *J Cell Sci* 2016; **129**:3026–3041.
37. Tsujikawa M, Malicki J. Intraflagellar transport genes are essential for differentiation and survival of vertebrate sensory neurons. *Neuron* 2004; **42**:703–716.
38. Crouse JA, Lopes VS, Sanagustin JT, Keady BT, Williams DS, Pazour GJ. Distinct functions for IFT140 and IFT20 in opsin transport. *Cytoskeleton (Hoboken)* 2014; **71**:302–310.
39. Xu M, Yang L, Wang F, Li H, Wang X, Wang W, Ge Z, Wang K, Zhao L, Li H, Li Y, Sui R et al. Mutations in human IFT140 cause non-syndromic retinal degeneration. *Hum Genet* 2015; **134**:1069–1078.
40. Chen SR, Batool A, Wang YQ, Hao XX, Chang CS, Cheng CY, Liu YX. The control of male fertility by spermatid-specific factors: searching for contraceptive targets from spermatozoon's head to tail. *Cell Death Dis* 2016; **7**:e2472.
41. Guzick DS, Overstreet JW, Factor-Litvak P, Brazil CK, Nakajima ST, Coutifaris C, Carson SA, Cisneros P, Steinkampf MP, Hill JA, Xu D, Vogel DL et al. Sperm morphology, motility, and concentration in fertile and infertile men. *N Engl J Med* 2001; **345**:1388–1393.
42. Lindemann CB, Lesich KA. Functional anatomy of the mammalian sperm flagellum. *Cytoskeleton (Hoboken)* 2016; **73**:652–669.
43. Pereira R, Sa R, Barros A, Sousa M. Major regulatory mechanisms involved in sperm motility. *Asian J Androl* 2017; **19**:5–14.
44. Ellinger I. The Calcium-Sensing Receptor and the Reproductive System. *Front Physiol* 2016; **7**:371.
45. Darszon A, Lopez-Martinez P, Acevedo JJ, Hernandez-Cruz A, Trevino CL. T-type Ca2+ channels in sperm function. *Cell Calcium* 2006; **40**:241–252.
46. Nguyen TM, Duittoz A, Praud C, Combarnous Y, Blesbois E. Calcium channels in chicken sperm regulate motility and the acrosome reaction. *FEBS J* 2016; **283**:1902–1920.
47. Naz H, Islam A, Ahmad F, Hassan MI. Calcium/calmodulin-dependent protein kinase IV: a multifunctional enzyme and potential therapeutic target. *Prog Biophys Mol Biol* 2016; **121**:54–65.
48. Williams HL, Mansell S, Alasmari W, Brown SG, Wilson SM, Sutton KA, Miller MR, Lishko PV, Barratt CL, Publicover SJ, Martins da Silva S. Specific loss of CatSper function is sufficient to compromise fertilizing capacity of human spermatozoa. *Hum Reprod* 2015; **30**:2737–2746.
49. Ernesto JI, Weigel Munoz M, Battistone MA, Vasen G, Martinez-Lopez P, Orta G, Figueiras-Fierro D, De la Vega-Beltran JL, Moreno IA, Guidobaldi HA, Giojalas L, Darszon A et al. CRISP1 as a novel CatSper regulator that modulates sperm motility and orientation during fertilization. *J Cell Biol* 2015; **210**:1213–1224.
50. Darszon A, Beltran C, Felix R, Nishigaki T, Trevino CL. Ion transport in sperm signaling. *Dev Biol* 2001; **240**:1–14.
51. Miller MR, Mansell SA, Meyers SA, Lishko PV. Flagellar ion channels of sperm: similarities and differences between species. *Cell Calcium* 2015; **58**:105–113.
52. Singh AP, Rajender S. CatSper channel, sperm function and male fertility. *Reprod Biomed Online* 2015; **30**:28–38.
53. Santi CM, Orta G, Salkoff L, Visconti PE, Darszon A, Trevino CL. K+ and Cl- channels and transporters in sperm function. *Curr Top Dev Biol* 2013; **102**:385–421.
54. Lishko PV, Kirichok Y, Ren D, Navarro B, Chung JJ, Clapham DE. The control of male fertility by spermatozoan ion channels. *Annu Rev Physiol* 2012; **74**:453–475.
55. Darszon A, Nishigaki T, Beltran C, Trevino CL. Calcium channels in the development, maturation, and function of spermatozoa. *Physiol Rev* 2011; **91**:1305–1355.
56. Hildebrand MS, Avenarius MR, Fellous M, Zhang Y, Meyer NC, Auer J, Serres C, Kahrizi K, Najmabadi H, Beckmann JS, Smith RJ. Genetic male infertility and mutation of CATSPER ion channels. *Eur J Hum Genet* 2010; **18**:1178–1184.
57. Carr DW, Newell AE. The role of A-kinase anchoring proteins (AKaps) in regulating sperm function. *Soc Reprod Fertil Suppl* 2007; **63**:135–141.
58. Yeung CH, Barfield JP, Cooper TG. The role of anion channels and Ca2+ in addition to K+ channels in the physiological volume regulation of murine spermatozoa. *Mol Reprod Dev* 2005; **71**:368–379.
59. Yeung CH, Barfield JP, Cooper TG. Chloride channels in physiological volume regulation of human spermatozoa. *Biol Reprod* 2005; **73**:1057–1063.
60. Barfield JP, Yeung CH, Cooper TG. Characterization of potassium channels involved in volume regulation of human spermatozoa. *Mol Hum Reprod* 2005; **11**:891–897.
61. Luconi M, Cantini G, Baldi E, Forti G. Role of a-kinase anchoring proteins (AKAPs) in reproduction. *Front Biosci (Landmark Ed)* 2011; **16**:1315–1330.
62. Agarwal A, Saleh RA, Bedaiwy MA. Role of reactive oxygen species in the pathophysiology of human reproduction. *Fertil Steril* 2003; **79**:829–843.
63. Ford WC. Regulation of sperm function by reactive oxygen species. *Hum Reprod Update* 2004; **10**:387–399.
64. O'Flaherty C. Redox regulation of mammalian sperm capacitation. *Asian J Androl* 2015; **17**:583–590.

65. Lavranos G, Balla M, Tzortzopoulou A, Syriou V, Angelopoulou R. Investigating ROS sources in male infertility: a common end for numerous pathways. *Reprod Toxicol* 2012; **34**:298–307.
66. de Lamirande E, O'Flaherty C. Sperm activation: role of reactive oxygen species and kinases. *Biochim Biophys Acta* 2008; **1784**:106–115.
67. Yeung CH, Anapolski M, Sipila P, Wagenfeld A, Poutanen M, Huhtaniemi I, Nieschlag E, Cooper TG. Sperm volume regulation: maturational changes in fertile and infertile transgenic mice and association with kinematics and tail angulation. *Biol Reprod* 2002; **67**: 269–275.
68. Rossato M, Balercia G, Lucarelli G, Foresta C, Mantero F. Role of seminal osmolarity in the reduction of human sperm motility. *Int J Androl* 2002; **25**:230–235.
69. Gaskell A, Crennell S, Taylor G. The three domains of a bacterial sialidase: a beta-propeller, an immunoglobulin module and a galactose-binding jelly-roll. *Structure* 1995; **3**:1197–1205.
70. Snook CF, Jones JA, Hannun YA. Sphingolipid-binding proteins. *Biochim Biophys Acta* 2006; **1761**:927–946.
71. Levental I, Veatch SL. The continuing mystery of lipid rafts. *J Mol Biol* 2016; **428**:4749–4764.
72. George KS, Wu S. Lipid raft: a floating island of death or survival. *Toxicol Appl Pharmacol* 2012; **259**:311–319.
73. Trevino CL, Serrano CJ, Beltran C, Felix R, Darszon A. Identification of mouse trp homologs and lipid rafts from spermatogenic cells and sperm. *FEBS Lett* 2001; **509**:119–125.
74. Travis AJ, Merdiushev T, Vargas LA, Jones BH, Purdon MA, Nipper RW, Galatioto J, Moss SB, Hunnicutt GR, Kopf GS. Expression and localization of caveolin-1, and the presence of membrane rafts, in mouse and Guinea pig spermatozoa. *Dev Biol* 2001; **240**: 599–610.
75. Zhu L, Inaba K. Lipid rafts function in Ca2+ signaling responsible for activation of sperm motility and chemotaxis in the ascidian Ciona intestinalis. *Mol Reprod Dev* 2011; **78**:920–929.
76. Jenkins PM, Hurd TW, Zhang L, McEwen DP, Brown RL, Margolis B, Verhey KJ, Martens JR. Ciliary targeting of olfactory CNG channels requires the CNGB1b subunit and the kinesin-2 motor protein, KIF17. *Curr Biol* 2006; **16**:1211–1216.
77. Qin H, Burnette DT, Bae YK, Forscher P, Barr MM, Rosenbaum JL. Intraflagellar transport is required for the vectorial movement of TRPV channels in the ciliary membrane. *Curr Biol* 2005; **15**:1695–1699.
78. Loreng TD, Smith EF. The central apparatus of cilia and eukaryotic flagella. *Cold Spring Harb Perspect Biol* 2017; **9**:a028118.
79. Mitchell DR. Speculations on the evolution of 9+2 organelles and the role of central pair microtubules. *Biol Cell* 2004; **96**:691–696.
80. Irons MJ, Clermont Y. Kinetics of fibrous sheath formation in the rat spermatid. *Am J Anat* 1982; **165**:121–130.
81. Eddy EM, Toshimori K, O'Brien DA. Fibrous sheath of mammalian spermatozoa. *Microsc Res Tech* 2003; **61**:103–115.
82. Eddy EM. The scaffold role of the fibrous sheath. *Soc Reprod Fertil Suppl* 2007; **65**:45–62.
83. Marshall WF. Basal bodies platforms for building cilia. *Curr Top Dev Biol* 2008; **85**:1–22.
84. Lehti MS, Sironen A. Formation and function of the manchette and flagellum during spermatogenesis. *Reproduction* 2016; **151**:R43–R54.
85. Kierszenbaum AL. Intramanchette transport (IMT): managing the making of the spermatid head, centrosome, and tail. *Mol Reprod Dev* 2002; **63**: 1–4.
86. Sironen A, Hansen J, Thomsen B, Andersson M, Vilkki J, Toppari J, Kotaja N. Expression of SPEF2 during mouse spermatogenesis and identification of IFT20 as an interacting protein. *Biol Reprod* 2010; **82**:580–590.
87. Young SA, Miyata H, Satouh Y, Aitken RJ, Baker MA, Ikawa M. CABYR is essential for fibrous sheath integrity and progressive motility in mouse spermatozoa. *J Cell Sci* 2016; **129**:4379–4387.
88. O'Donnell L, Nicholls PK, O'Bryan MK, McLachlan RI, Stanton PG. Spermiation: The process of sperm release. *Spermatogenesis* 2011; **1**:14–35.